AIMS Materials Science, 6(6): 911–943.
DOI: 10.3934/matersci.2019.6.911
Received: 11 July 2019
Accepted: 16 September 2019
Published: 17 October 2019

http://www.aimspress.com/journal/Materials

Research article

Nanotechnological characterization of allofanite and faujasite (Y-faujasite) catalysts and comparing with a commercial FCC catalyst (X-zeolite)

Edward Jiménez*, Santiago Lalangui, Edison Guacho, Ana Emperatriz Paucar, Paulina Herrera, David Vaca, Humberto González, Patricia Ochoa, Ullrich Stahl and Gustavo López

Faculty of Chemical Engineering, Central University of Ecuador, Quito 170521, Ecuador

* **Correspondence:** Email: ehjimenez@uce.edu.ec; Tel: +5932524766.

Abstract: We studied the synthesis variables of the faujasite using natural clinker of the Cotopaxi volcano, and allophane (allofanite) from the province of Santo Domingo de los Tsachilas as raw materials, as well as their physicochemical properties and their influence on the catalytic efficiency for Ecuadorian oil and asphalt.

The synthesized materials were subjected to laboratory tests, like thermogravimetric characterization, BET area, FTIR, chemisorption and AFM. Tests of catalytic activity in crude oil and asphalt with different °API and percentage of Sulfur showed ranges of optimal efficiency. These ranges contributed to obtain a logistic regression model with min. 90% accuracy, which was entered into a confusion matrix. This function can be optimized in the intervals of each of the variables of any refinery.

It is concluded that the logistic regression model for catalytic efficiency is sensitive to changes in the amount of faujasite and allophane (allofanite) in the catalytic cracking process. In the same way, a fundamental dependence of the surface area (BET) was found, which for the case of allophane is formed in contribution of each of the nanopores whose size is in the order of 3 to 5 nm, while the faujasite has nanopore sizes from 17 to 35 nm.

Keywords: natural clinker; faujasite; allophane (allofanite); nanopores; catalytic efficiency; logistic regression

1. Introduction

Petroleum refining plays globally a very important role in our lives. The vast majority of transport vehicles as well as agricultural and industrial machinery use petroleum products such as diesel, gasoline, kerosene, fuel oil, etc.

Currently, due to the pollution generated by this type of fuels, certain laws have been established which regulate the quality of these, making them more efficient and with a lower content of contaminating substances such as sulphur, aromatic components, etc. It is for this reason that more and more efficient ways of producing better fuels are studied, such as improving the process of fluidized catalytic cracking (FCC) using new catalysts [1]. Another aspect is the necessity of the treatment of the spent catalysts, which generates a great environmental problem and elevated costs, as the spent catalyst is returned to the catalyst supplier companies.

One type of the catalysts most used in the catalytic cracking process has undoubtedly been the zeolites, which since its introduction in the 1940s have been the bases of important improvements in the performance of gasoline and octane, as well as in the production of fuels and cleaner lubricants [2]. The key ingredient in the success of this process has been the application of zeolites, especially the faujasites, as the catalytically active component in cracking catalysts [3].

The ability of small amounts of ZSM-5 added to the FCC unit to improve gasoline octane rating while producing more light olefins has prompted a substantial amount of process and catalyst research into zeolite-based FCC additives [4,5]. Zeolite catalysts used efficiently in petroleum refining processes are available in a text by Chen et al. [6] and in the articles by Chen and Degnan [7], Ruthven and Post [8], Connor et al [9] and Stoecker [10]. The development of improved FCC catalysts constitutes an interesting case study of the merits of selectively modifying a single crystal structure to achieve multiple catalytic targets [11]. Modifications in zeolite Y have continued to improve the selectivity of gasoline and octane [12].

A study of the physico-chemical properties of allophane compared to imogolite indicates the mineral form of two aluminosilicate allophanes, concluding that allophanes are more difficult to identify due to their variable structure. In addition, these two aluminosilicates have a high concentration of Si and Al in soil solutions, which is why IR spectroscopy is used as a technique to quantify them in the soil [13].

An important contribution to the composition and texture of an allophane as an aluminosilicate is its aluminum/silicon ratio (Al/Si), since, if the Al/Si ratio increases, the allophanic materials are successively developed [14]. Silicon (Si) is a transcendental component in the formation of allophanes. The main catalyst used in an FCC reactor is the active component Y-zeolite, which has an average particle size of 75 μm and an average surface area of 800 m^2/g. This aluminosilicate has a Y-faujasite structure, with the highest pore size of 0.8 nm, which is called the super cage. Its size allows some C18–C25 mono-, di- and tri-nuclear aromatics present in the Vacuum Gas Oil (VGO) to pass [15].

On the other hand, allophane is known to have an amorphous mineral structure consisting mainly of volcanic ash. Chemically it is a hydrated aluminosilicate with the formula $Al_2O_3 \cdot (SiO_2)_{1.3–2} \cdot (2.5–3)H_2O$. Its particle size is in the range from 3 to 5 nm, and shows a high specific surface area [16]. Based on these characteristics, it is suggested in this paper that allophane could be used as a catalyst substitute in the FCC process, since it may behave similarly to the commercial catalysts described above because they physically and chemically share similarity with

the main properties that characterise Zeolites used in FCC.

In summary, this article is oriented to carry out an in-depth study on the use of faujasite and allophane as catalysts in the fluidized catalytic cracking, mainly to determine the catalytic efficiency in the process. In particular, the Ecuadorian allophane, of which gigantic deposits in the order of 4000 km^2 were detected [17], has to be tested, which would be forcing the Ecuadorian research to give it the necessary importance, since it would be a technically and economically viable alternative for the local refining industry and worldwide.

2. Materials and method

2.1. Chemical activation

Catalyst samples of both faujasite and allophane obtained from the Cotopaxi volcano and from the province of Santo Domingo de los Tsachilas respectively, these samples followed the standard alkaline method. For this purpose, the samples of faujasite and allophane were calcined with sodium hydroxide (NaOH at 99.9% w/w, reactive grade in scale form) at 600 °C, 1h, at a ratio = 1.2 g NaOH/1 sample. From this process a solid and homogeneous sample of activated material with a very high alkalinity is obtained. To reduce its pH, we used distilled water Type 2 (electrical resistivity = 1 MΩ-cm, electrical conductivity = 3 μS/cm), until a neutral pH is obtained [18]. The other commercial catalyst used to compare its efficiency against activated samples was donated by the DEPEC laboratory (Department of Petroleum Energy and Pollutants) of the Faculty of Chemical Engineering of the Central University of Ecuador.

2.2. Catalyst characterization

The analysis of Fourier Transform Infrared Spectroscopy (FTIR) was performed with a Perkinelmer equipment, model L1600301 Spectrum Two Lita, which uses potassium bromide (KBr 99.9% w/w) as a solid plate containing the sample. The BET surface area analysis was performed in a SA-9603, 3 STATION, MULTI-POINT (HORIBA INSTRUMENTS INC.) equipment, which is based on a kinetic model of the monolayer adsorption process proposed in 1916 by Langmuir, which takes into account the formation of multilayers. To ensure total elimination of water in the sample, a pre-treatment of 300 °C was carried out in the same equipment for 90 min, once that the equipment was calibrated with altitude and ambient pressure, the sample is bathed with nitrogen at a temperature of −192 °C, so that it can absorb and desorb.

2.3. Methods

2.3.1. Allophane sample collection

Following the bibliography about the massive deposits of allophane in Ecuador located in the Province of Santo Domingo [19], three samples of raw material were taken with the assistance of the geologists of INIGEMM (National Institute of Geological Mining and Metallurgical Research), are shown in Table 1.

Table 1. GPS coordinates of the allophane deposits location.

Sample	Coding	Latitude	Longitude
1	SD-001	−0.162793	−79.078062
2	SD-002	−0.138647	−79.078362
3	SD-003	−0.203163	−79.091027

2.3.2. Preparation of allophane samples

These samples contain a high percentage of humidity due to their hygroscopic properties. As the analysis of allophane should be done on a dry basis, the samples were subjected to heating for 24 h at a temperature of 60 °C. The dry material was reduced in particle size using a cutting mill (SM 300, Retsch) employing a filter with 1 mm mesh at a speed of 1500 rpm.

2.3.3. Activation of the samples

For the formation of the active centers of the sample, the steps of activation of the method used for zeolites (alkaline fusion) were followed. This procedure is similar for both types of material, faujasite and allophane:

1. Mixing the dry and granulated sample with a strong base (in this case NaOH), in a ratio of 1.2 g of base per gram of sample.
2. Calcination of the sample at a temperature of 600 °C for 1 h.
3. Mixing 10 g of the calcined sample and 50 ml of distilled water type 1.
4. Stirring during 1 h at a speed of approximately 800 rpm for the allophane, and 1200 rpm for the faujasite, until the sample is homogenized and reduced to a small particle diameter.
5. The homogenized sample is placed in a Teflon tube inside a calorimeter (PARR INSTRUMENT CO. MOLINE ILL, USA. PATENT: 2065870. CODE: 101A 6938) adapted to keep the temperature of the sample constant.
6. The calorimeter with the sample inside is left at room temperature at different experimental times for the crystallization reaction to take place. These times were 1, 2, 3 and 4 d of ageing time.
7. After the ageing time has elapsed, the different samples are heated in an oven to 80 °C for different intervals of time, at 6, 12, 18, 24 and 30 h to complete the activation process.

2.3.4. FTIR-analysis

This analysis was performed with the PerkinElmer FT-IR Spectrometer Spectrum Two equipment. A defined amount of the synthesized product was homogeneously ground with potassium bromide (KBr) in a ratio of 1 to 100 and a translucent tablet was prepared.

2.3.5. Specific surface (BET)

This analysis was performed with the HORIBA SA 9600 SURFACE AREA ANALYSIS equipment. The determination of the specific area's highest value of the samples was considered as a parameter to establish the optimum time of activation in the hydrotreatment process and the time of aging.

2.3.6. Thermogravimetric analysis

This analysis was performed using a TGA 1 STARe System METTLER TOLEDO thermogravimetric balance. For our study we considered two types of crude oil, light (24.9 °API) for faujasite and allophane and asphalt (14.04 °API) for allophane alone. As a reference point, the thermogravimetry was analyzed with an inert atmosphere of N_2 to demonstrate the effect of the synthesized catalyst on the light crude oil and asphalt. The procedures for the two samples were as follows:

1. Insert in the TGA equipment a small amount of crude, between 20 and 30 mg.
2. Configure a dynamic analysis from 25 to 650 °C in the Equipment Software to analyze the temperatures where the highest degree of decomposition is evident. According to the behavior of the curve it is possible to show the temperatures that present the highest rate of decomposition.
3. At the temperatures with the highest decomposition rate of the light crude oil sample without allophane and faujasite, a dynamic analysis of 25 °C was set up to the reaction temperature determined at the previous literal, with a ramp of 10 °C/min, followed by an isothermal analysis of 30 min. The same procedure as above was repeated if there was more than one reaction temperature.
4. The procedure 3 was repeated by combining 3 types of samples: light crude oil with synthesized faujasite in a range of 0.02 to 0.07 g FAU/g crude oil, light crude oil with activated allophane at a ratio of 5% w/w, and asphalt with activated allophane at a ratio of 5% w/w.

2.3.7. X-ray diffraction analysis

This analysis was performed using a PHASER D2 Diffractometer which identifies the percentage of mineral present in the sample. Once generated the diffractogram that belongs to the sample, the mineral present are identified.

3. Results

3.1. Characterization of the synthesized faujasite

3.1.1. X-ray diffraction (XRD) analysis

In Figure 1, the X-ray diffractogram of the synthesized faujasite (FAU) is shown. Its composition is described as faujasite-Ca = 52.05%; Heulanndite-Ca = 8.34%; Orthodase = 28.87%; Pyrite = 2.89%; Limnite = 1.46%; Albite = 5.39%.

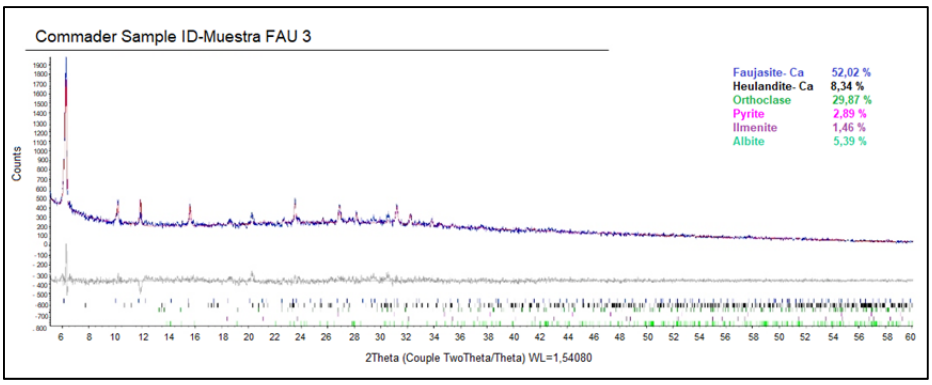

Figure 1. X-ray diffractogram of the synthesized faujasite sample.

The results of the diffractometry analysis of the faujasite are shown in Table 2 and gave information about the structural information of the unit cell and the number of TO_4 tetrahedra (T = Si, Al) per cell.

Table 2. Structural analysis of the synthesized faujasite.

Description	Value
Phase name	faujasite-Ca
R-Bragg	1.882
Spacegroup	227:02:00
Scale	1.97E-08
Cell mass	13184.706
Cell volume ($Å^3$)	15541.56
Wt%-Rietveld	52.02
Double–Voigt approach	
Cry size Lorentzian	69.3
k: 1 LVol-IB (nm)	44.091
k: 0.89 LVol-FWHM (nm)	61.639
Crystal linear absorption coeff (1/cm)	72.289
Crystal density (g/cm^3)	1.417
Preferred orientation (Dir 1: 3 3 1)	0.4356778
Preferred orientation (Dir 2: 5 3 3)	0.0452066
Fraction of Dir 1	0.995524
Lattice parameters	
A (Å)	24.90715

3.1.2. Atomic force microscopy (AFM) analysis

The AFM results for the faujasite synthesized from the natural clinker are shown in Figure 2, in which the following views A-D can be appreciated. At the bottom of the figure, a curve is shown in which its concave sections represent the pores of the synthesized faujasite. The color identification

box shows the pore sizes represented by the distance between the colored lines.

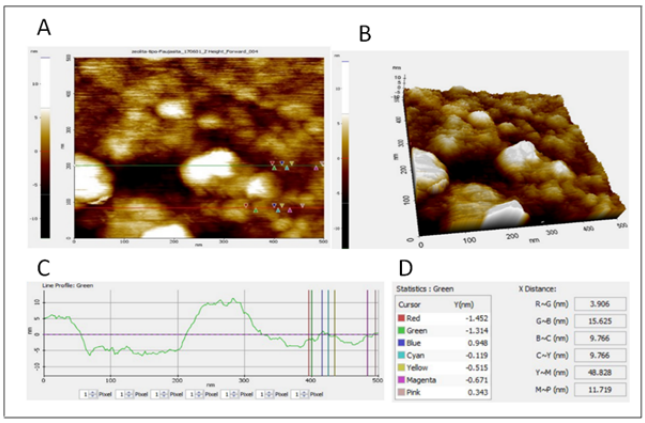

Figure 2. AFM analysis of the synthesized faujasite. (a) 2D top-view of the synthesized faujasite. (b) 3D view of the synthesized faujasite. (c) identification of the pores of the synthesized faujasite. (d) values corresponding to the pore size of the synthesized faujasite.

3.1.3. Fourier transform infrared spectroscopy (FT-IR) analysis

The FT-IR analysis was carried out for the synthesized faujasite and the new acquired FCC catalyst (catalyst used in Ecuador at the Esmeraldas State Refinery). The corresponding spectra are shown in Figure 3. The comparison of both spectra showed that the synthesized faujasite contains the main functional groups of the zeolithic catalysts used in the refinery.

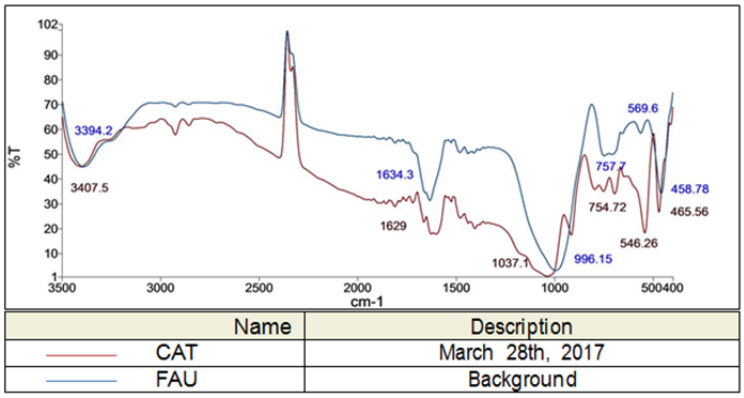

Figure 3. Infrared spectrum for synthesized faujasite (blue) and acquired FCC catalyst (red).

Transmittance peaks at different wavelengths are shown, which represent the characteristic functional groups present in the synthesized faujasite and the zeolite used in the FCC reactor. The values of the peaks representing the functional groups contained in the samples are interpreted in Table 3, showingthe main functional groups present in the synthesized faujasite in comparison with the acquired FCC catalyst, depending on the transmittance obtained.

Table 3. Interpretation of the IR spectrum for the synthesized faujasite and the new FCC catalyst. For the samples, the wavelength and % Transmittance is shown as well as the interpretation of the respective peak.

Location of peaks in the IR spectrum (cm^{-1})		Peak interpretation
Synthesized faujasite (FAU)	Acquired FCC catalyst	
Approx. 3394.2; 44%	Approx. 3407.5; 44%	Vibration of water molecules, OH groups
Approx. 1634.3; 35%	Approx. 1634.3; 21%	Deformation mode of H_2O
Approx. 996.15; 10%	Approx. 1037.1; 1%	Asymmetric stretch T-O (T = Si or Al)
Approx. 757.7; 50%	Approx. 754.7; 38%	Symmetrical stretch T-O (T = Si or Al)
Approx. 569.6; 41%	Approx. 546.2; 32%	Double rings (D4R, D6R)
Approx. 458.78; 38%	Approx. 465.5; 30%	Presence of the supercage

3.1.4. Particle size distribution

The particle size of the synthesized faujasite and the acquired FCC catalyst were compared to corroborate whether they have a similar behavior in a dynamic scenario like a FCC process. The size distribution is shown in Figure 4. It was evidenced that both samples have a similar size distribution.

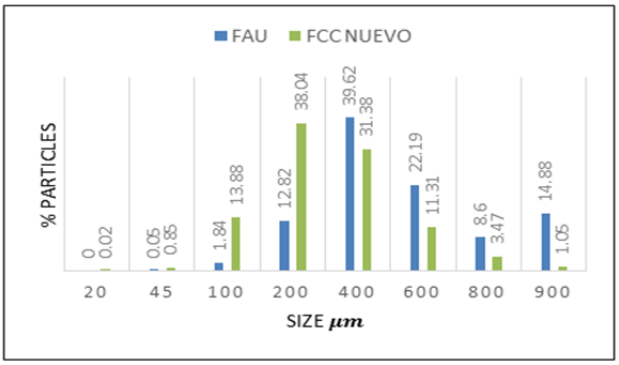

Figure 4. Particle size distribution for the acquired FCC and the faujasite catalyst.

For the synthesized faujasite, the surface area and its pore volume were analyzed, for which three tests were carried out and the average of these values was taken, which is shown in Table 4.

Table 4. Results of BET area for synthesized faujasiteand pore volume tests.

Test	Superficial area (BET) (m^2/g)	Pore volume (mL/g)
1	360.46	0.2137
2	347.43	0.2051
3	362.16	0.2159

The average value of the synthesized faujasite surface area was 356 m^2/g and the average pore volume was 0.2115 ml/g. This value was compared with the theoretical values of type Y zeolite, which is commercially used in the FCC unit [20], as shown in Table 5.

Table 5. Comparison of surface area and pore volume of the synthesized faujasite and the acquired zeolite type Y.

Sample	Superficial area (BET) (m^2/g)	Pore volume (mL/g)
Synthesized faujasite	356.68	0.2116
Acquired FCC catalyst (zeolite type Y)	218.66	0.2360

It was evident that the synthesized faujasite had a larger surface area and a smaller pore volume compared with the acquired FCC catalyst.

3.1.5. Thermogravimetric analysis

The data obtained from the thermobalance were expressed as percentage of loss of crude oil mass as a function of time. The catalytic cracking zone in the thermogravimetric curves from 10 to 45 min, correlated with a temperature interval from 300 to 350 °C are presented in Figure 5. The area under the curve was determined by the trapezoid method.

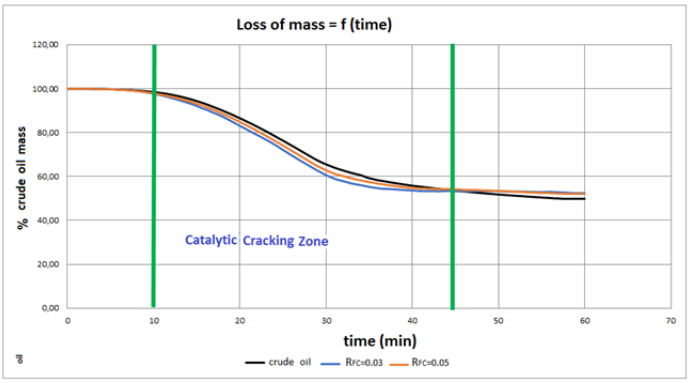

Figure 5. Graphical representation of the percentage of mass loss of crude oil vs. analysis time.The catalytic cracking zone is represented between the green lines from 10 to 45 min, performed for crude oil without catalyst (black curve), crude oil with 3% w/w faujasite (blue curve) (R_{FC} = 0.03g FAU/g crude oil) and crude oil with 5% w/w faujasite (orange curve) (R_{FC} = 0.05 g FAU/g crude oil).

The calculations were then performed using Eq 1, determining the percentage of the mass loss of crude oilin the TGA process using crude oil without catalyst and crude oil with faujasite at 3% w/w and 5% w/w. The data obtained are tabulated in Table 6.

$$\%m_{crudeoil} = 100 - \frac{M_{initial} - M_{final}}{M_{initial}} \times 100 \quad (1)$$

where $\%m_{crudeoil}$ = percentage of the mass loss of crude oil; $M_{initial}$ = mass of crude oil mixed with synthesized faujasite before the TGA analysis; M_{final} = mass of crude oil mixed with synthesized faujasite after TGA analysis.

Table 6. Crude oil mass loss in percentage for R_{FC} = 0.03 y R_{FC} = 0.05.

Time (min)	Crude oil (%m)	R_{FC} = 0.03 (g FAU/g crude oil) (%m)	R_{FC} = 0.05 (g FAU/g crude oil)(%m)
10	98.664	98.023	98.154
12	97.345	95.856	96.452
15	94.406	92.169	93.211
17	91.023	88.305	89.594
20	85.888	82.299	84.134
23	79.909	75.987	77.794
25	76.010	73.707	71.642
28	69.208	64.511	66.643
30	65.648	60.613	62.920
32	62.364	59.791	57.399
35	58.988	54.940	57.262
37	57.650	54.256	56.109
40	55.827	53.565	54.870
45	53.673	53.188	54.127

The crude oil mass loss percentages are shown for each of the samples used in the TGA process as a function of the analysis time.

The catalytic cracking zone for light crude oil with faujasite is the area under the curve determined by the numerical integration method (Simpson method 3/8), represented in the Eq 2, and shown in Table 7.

$$A = \frac{3}{8}h[f(x_0) + 3f(x_1) + 3f(x_2) + f(x_3)] \quad (2)$$

$$h = \frac{b-a}{n} \quad (3)$$

$$E_{(f)} = \frac{n}{80}h^5 f^{iv}(\xi) \quad (4)$$

where A = area under the curve; n = 59; a and b = limits of variation in mass; $f(xi)$ = time variation; $E_{(f)}$ = numerical method error; $f^{iv}(\xi)$ = fourth derivative of the function of the thermogravimetric curves evaluated at the maximum value of the interval [a,b].

Once the catalytic cracking zone was determined, the percentage recovery of light compounds was calculated and represented in Table 6.

$$\%R = \frac{A_{SF} - A_{CF}}{A_{SF}} \times 100 \quad (5)$$

Where $\%\ R$ = Percentage of recovery of light compounds; ASF = Area under the curve in the cracking zone for crude oil without faujasite; ACF = Area under the curve in the cracking zone for crude oil with faujasite.

The percentage of mass recovery of crude oil at the two different faujasite/crude ratios is shown in Table 7, obtaining the highest percentage of light compounds recovered at a 5% ratio of faujasite in the crude oil sample. The error percentage refers to the error obtained by comparing the result of

the area under the curve between the Simpson method and the integration method by regression obtained from the curves.

Table 7. Total areas and recovery of light compounds for the ratios of 0.03 and 0.05 g FAU/g crude oil.

Sample	Total area	%Error	%R
Crude without faujasite	2545.64	-9.96×10^{-4}	-
$R_{FC} = 0.03$	2435.39	-1.84×10^{-3}	2.21
$R_{FC} = 0.05$	2489.29	-1.94×10^{-3}	4.33

3.2. Characterization of allophane

3.2.1. X-ray diffraction (XRD) analysis

The analysis of X-ray diffraction of the 3 different sampling sites gives the composition of the main mineralogical structures contained in the allophane sample without treatment, shown in Table 8. The determination of the components with crystallization defined in the samples was carried out using a PHASER D2 Diffractometer, using Difrac plus software for measurement, EVA and TOPAS 4.2 for the identification and quantification of the crystalline phases present in each of the samples. The numbering of the tests carried out in the XRD analysis represent the different samples, the correlation to their sampling location coordinates can be seen in Table 1.

Table 8. X-ray diffraction results for allophane for the three different samples.

Mineral	Formula	Test SD-001 (%P/P)	Test SD-002 (%P/P)	Test SD-003 (%P/P)
Sanidine	$(K,Na)(Si,Al)_4O_8$	26.78	14.93	19.39
Cristobalite	SiO_2	23.43	26.89	18.77
Anorthite	$CaAl_2Si_2O_8$	11.49	7.56	9.76
Pargasite	$NaCa_2(Mg_4Al)\ (Si_6Al_2)O_{22}(OH)_2$	10.69	13.81	10.71
Quartz	SiO_2	8.16	16.45	24.07
Andesine	$(Na,Ca)(Si,Al)_4O_8$	8.07	13.82	7.26
Cordierite	$(Mg,Fe)_2Al_4Si_5O_8$	4.31	4.49	4.23
Albite	$NaAlSi_3O_8$	3.80	-	-
Sylvite	KCl	2.45	-	-
Vermiculite	$(Mg,Ca)_{0.7}(Mg,Fe,Al)_6\ [(Al,Si)_8O_{20})](OH)_4.8H_2O$	-	-	3.88
Trace components	-	0.82	-	1.93

3.2.2. Atomic force microscopy (AFM) analysis

The AFM results for allophane for both the non-activated sample and the sample activated by the alkaline fusion process are shown in Figures 6 and 7 respectively. Both figures show a 2D-representation (a), a 3D-representation (b), an identification of the nanopores (c) and their size (d) for the allophane.

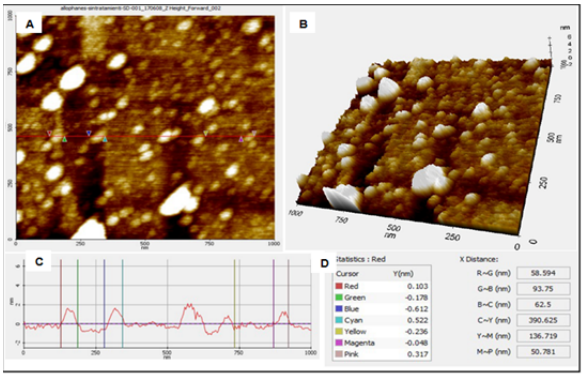

Figure 6. Pure allophane AFM test. (a) 2D view of allophane, (b) 3D view of allophane, (c) identification of allophane nanopores, (d) values corresponding to the size of the nanopores of allophane.

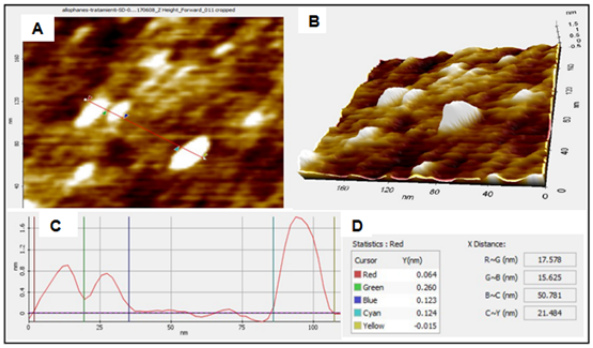

Figure 7. Activated allophane AFM analysis. (a) 2D view of allophane, (b) 3D view of allophane, (c) identification of allophane nanopores, (d) values corresponding to the size of allophane nanopores.

3.2.3. Fourier transform infrared spectroscopy (FT-IR) analysis

The FT-IR analysis was performed for the natural and the activated allophane, shown in Figures 8 and 9 respectively.

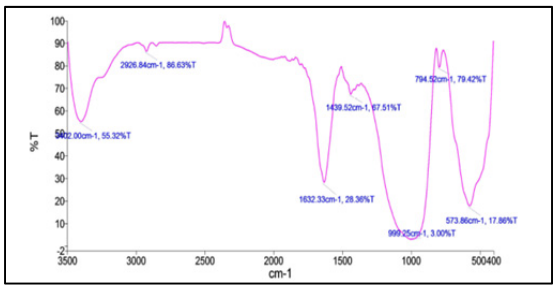

Figure 8. IR spectrum for the pure allophane (without activation process). Corresponding spectra of the major functional groups are shown.

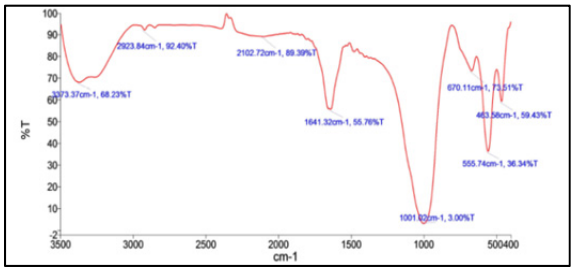

Figure 9. IR spectrum for the activated allophane (using the alkaline fusion process). Corresponding spectra of the major functional groups are shown.

The peak values which represent the functional groups contained in the samples are interpreted in Table 9, the peaks and their respective transmittance are given.

From the experiments carried out we took into consideration the representative samples in surface area because no change in their structure was evidenced.

Table 9. Interpretation of the allophane spectra analyzed with the FTIR.

Location of peaks in the IR spectrum (cm^{-1})		Interpretation
Pure allophane	Activated allophane	
Approx. 3402; 55%	Approx. 3373; 68%	Vibration of water molecules, OH groups
Approx. 2926; 86%	Approx. 2923; 92%	Alkanes (CH_3, CH_2 and CH), alkynes, mercaptanes
	Approx. 2102; 39%	Functional groups -N=C=S
Approx. 1632; 36%	Approx. 1641; 55%	Vibration of carbon molecules in C=C, C=O groups belonging to coke
Approx. 1439; 67%		Vibration of functional groups C=N
Approx. 999; 3%	Approx. 1001; 3%	Spectrum belonging to V^{5+}, V=O
Approx. 794; 79%		Spectrum belonging to V^{5+}, asymmetric V-OV and CH
	Approx. 670; 73%	Vibration belonging to functional group C-I
Approx. 573; 17%	Approx. 555; 36%	Vibration pertaining to C–C bonds
	Approx. 463; 59%	Spectrum belonging to SO_2

3.2.4. Surface area (BET) analysis

The BET surface area tests were performed on the 3 samples, each at different activation times, as shown in the Table 10.

Table 10. Surface area vs. hydrotreatment time for 3 different allophane samples.

Sample	Pure allophane	Hydrotreatment time					
		6 h	12 h	18 h	24 h	30 h	
SD-001	357.9	193.6	181.1	234.0	141.2	153.8	Area (m^2)
SD-002	355.6	163.2	106.6	192.2	179.0	173.7	
SD-003	250.6	290.1	287.9	445.2	361.3	383.6	

It was evidenced that at an activation time superior to 6 h, the surface area tended to increase to a maximum value, which was taken as the optimum time of hydrotreatment (18 h) and decreased with extended treatment (see Figure 10).

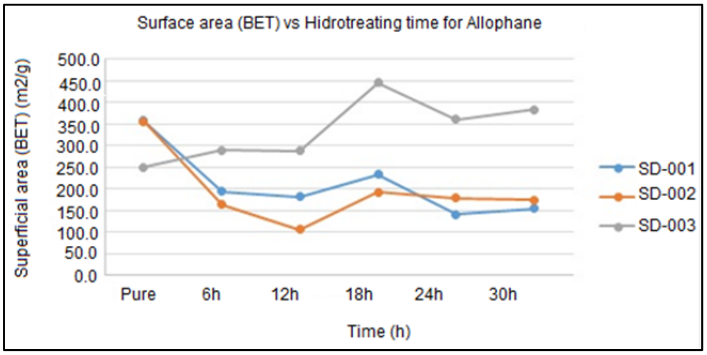

Figure 10. Comparison of surface area curves as a function of hydrotreatment time for allophane. The different samples are identified as SD-001, SD-002 and SD-003.

3.2.5. Thermogravimetric analysis

In order to determine the reaction temperatures of both light crude oil and asphalt a dynamic process was carried out in the software, analyzing its behavior in an interval from 25 to 650 °C. In Figure 11 this is shown for light crude oil and in Figure 12 for asphalt. Its behavior is observed and it helps to determine the main reaction temperature. The best reaction temperature was analyzed which helped to evaluate the behavior of the catalyst.

Although its maximum disintegration temperature is 480 °C, the asphalt started to boil before reaching this temperature, causing vibrations and thus erroneous TGA data, leading to deviations. According to the behavior that was presented in the dynamic analysis of crude and asphalt, we take the following reaction temperatures tabulated in Table 11 to analyze the efficiency of allophane as a catalyst.

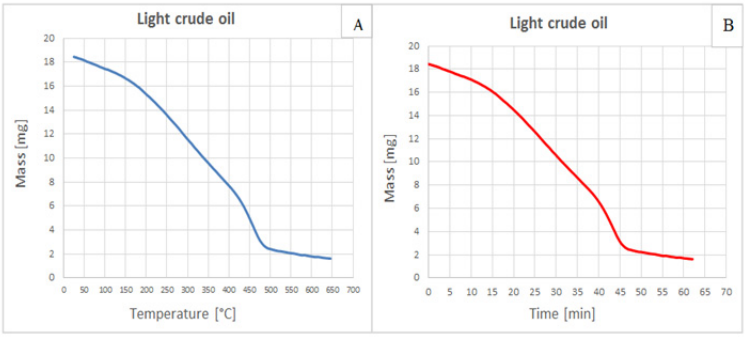

Figure 11. Evolution of the dynamic process of light crude oil in the TGA analysis. (a) dynamic analysis of light crude oil as a function of temperature, (b) dynamic analysis of light crude oil as a function of time.

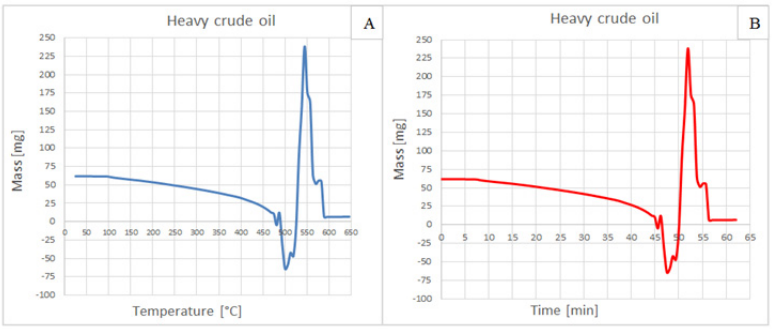

Figure 12. Evolution of the dynamic process for asphalt in the TGA analysis. (a) dynamic analysis of asphalt as a function of temperature, (b) dynamic analysis of asphalt as a function of time.

Table 11. Light crude oil and asphalt temperatures of reaction.

Sample	Reaction temperature (°C)
Light crude oil	150
	320
	420
Asphalt	420

For the analysis of light crude oil (ºAPI = 24.9) three temperatures are considered corresponding to the first signs of decomposition of the sample presented in Figure 13. Each of these has an isothermal analysis time of 30 min with a heating ramp of 10 °C/min, in an inert atmosphere of N_2(g). For asphalt (ºAPI = 13.9), its thermal cracking was analyzed at the reaction temperature of 420 °C (see Figure 14), which was the best approximation before it started to boil.

Both graphs show that the cracking of light crude oil with pure allophane and activated allophane improves notably compared to crude oil without catalyst and crude oil with FCC catalyst, because the area under the curve is smaller for cracking with pure and activated allophane. As well, for the cracking of asphalt, both graphs show a smaller area under the curve when using pure allophane, indicating an improvement in the decomposition process of the asphalt.

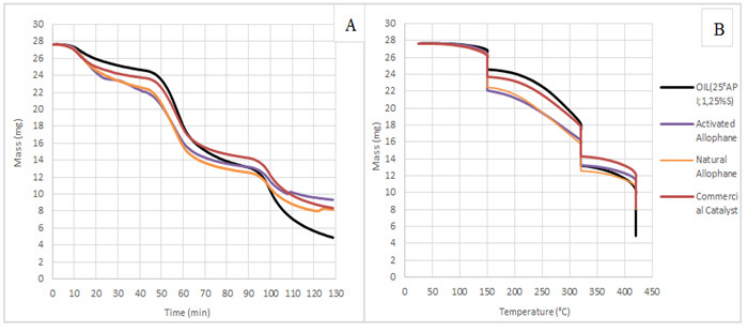

Figure 13. Results from TGA analysis for light crude oil at the temperatures determined in Table 14. (a) analysis of allophane's activity in the light crude oil cracking as a function of time, (b) analysis of allophane's activity in the light crude oil cracking as a function of the temperature.

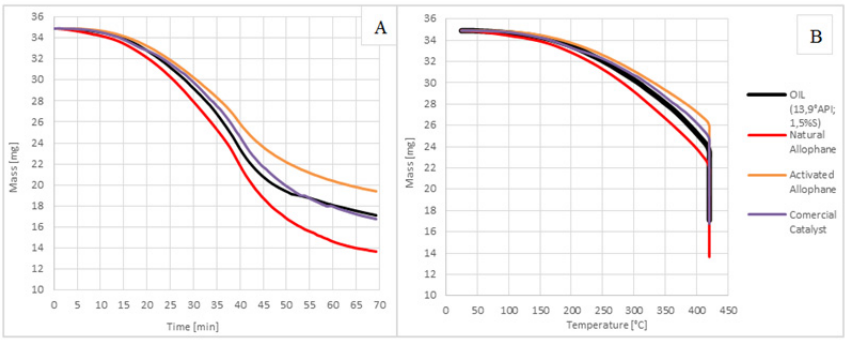

Figure 14. Results from TGA analysis for Asphalt at the temperature determined in Table 14. (a) analysis of allophane's activity for the Asphalt cracking as a function of time, (b) analysis of allophane's activity for the Asphalt cracking as a function of the temperature.

The samples analyzed in the TGA assay consisted of: activated allophane (the one with the highest surface area), allophane without activation process, zeolite used in the FCC Unit, and crude without catalyst. Of which 4 curves were obtained to compare their behavior and efficiency simulating the cracking process in an FCC reactor. From this process, the sample showing the best efficiency will be the one that has the smallest area under the curve in coordinates of mass vs. time, as shown in Figure 14a, and experimental values are shown in Table 12 for light crude oil and Table 13 for asphalt.

Table 12. TGA results for the different samples with light crude oil.

N	Time	Temperature	Oil (25 ºAPI; 1.2%S)	Activated allophane	Natural allophane	Commercial catalyst
	(min)	(°C)	Mass (mg)	Mass (mg)	Mass (mg)	Mass (mg)
1	0	25	27.641	27.641	27.641	27.641
2	5.2	77	27.616	27.626	27.564	27.5579
3	11.7	142	27.090	26.798	26.672	26.5749
4	18.2	150	26.129	24.792	24.954	25.2239
5	24.7	150	25.546	23.604	23.950	24.6079
6	31.2	150	25.113	23.349	23.277	24.1549
7	37.7	150	24.782	22.5431	22.753	23.8599
8	44.2	167	24.492	21.8629	22.3257	23.6159
9	50.7	232	23.255	20.1613	20.3713	22.3009
10	57.2	297	19.839	17.28915	17.0056	19.2019
11	63.7	320	16.505	15.1402	14.5759	16.5149
12	70.2	320	15.122	14.29882	13.6757	15.4859
13	76.7	320	14.204	13.78057	13.1582	14.9169
14	83.2	320	13.617	13.45235	12.8113	14.5529
15	89.7	322	13.177	13.22544	12.56215	14.2819

Continued on next page

N	Time (min)	Temperature (°C)	Oil (25 ºAPI; 1.2%S) Mass (mg)	Activated allophane Mass (mg)	Natural allophane Mass (mg)	Commercial catalyst Mass (mg)
16	96.2	387	12.102	12.5611	11.83645	13.5239
17	102.7	420	9.138	10.8247	9.99068	11.3179
18	109.2	420	7.274	10.2685	8.91915	9.9879
19	115.7	420	6.175	9.81255	8.31515	9.2109
20	122.2	420	5.427	9.5209	8.0247	8.7059
21	128.7	420	4.883	9.337901	8.1714	8.3559

*Note: Oil (25 ºAPI; 1.25% S): data of the TGA analysis of light crude oil without additives and the following properties: °API of 25 and 1.25%t of sulfur. Activated allophane: light crude with the addition of a sample of activated allophane. Natural allophane: light crude with addition of a sample of allophane in pure state. Commercial catalyst: light crude with addition of the commercial catalyst used in the FCC unit from the refinery (acquired FCC catalyst).

Table 13. TGA results for the different samples with asphalt.

N	Time (min)	Temperature (°C)	Oil (13.9 ºAPI; 2.6%S) Mass (mg)	Activated allophane Mass (mg)	Natural allophane Mass (mg)	Commercial catalyst Mass (mg)
1	0	25	24.060	21.460	34.904	19.888
2	2.8	53	24.038	21.453	34.863	19.873
3	6.3	88	23.920	21.419	34.753	19.801
4	9.8	123	23.714	21.270	34.413	19.562
5	13.3	158	23.369	20.957	33.896	19.143
6	16.8	193	22.765	20.438	33.125	18.453
7	20.3	228	21.879	19.724	32.088	17.745
8	23.8	263	20.804	18.815	30.785	16.899
9	27.3	298	19.512	17.729	29.184	15.757
10	30.8	333	18.015	16.512	27.297	14.429
11	34.3	368	16.339	15.187	25.042	12.865
12	37.8	403	14.191	13.664	22.327	11.027
13	41.3	420	11.728	11.719	18.977	8.666
14	44.8	420	10.010	10.238	16.551	6.770
15	48.3	420	8.913	9.157	14.825	5.433
16	51.8	420	8.229	8.324	13.466	4.333
17	55.3	420	7.863	7.646	12.348	5.523
18	58.8	420	7.367	7.089	11.464	4.828
19	62.3	420	6.977	6.654	10.728	4.449
20	65.8	420	6.602	6.272	10.129	3.987
21	69.3	420	6.255	5.953	9.605	3.622

*Note: Oil (13.9 ºAPI; 2.6% S): data of the TGA analysis of pure asphalt sample without additives, and the following properties: ºAPI of 13.9 and 2.6% of Sulfur. Activated allophane: asphalt with addition of an activated allophane sample. Natural allophane: asphalt with addition of a sample of allophane in its pure state. Commercial catalyst: asphalt with addition of the commercial catalyst used in the FCC unit from the refinery (acquired FCC Catalyst).

3.2.6. Chemisortion

The determination of the active sites of pure and activated allophane is represented in Tables 14 and 15. This contains the amount of ammonia adsorbed by the sample in the TPD test, in zones L and H that identify the acidity of Lewis and Brøsnted respectively.

Table 14. Results obtained from the TPD test of pure allophane.

Sample	Adsorption zone	Test 1	Test 2	Test 3
		Vol. NH_3 (cm^3/g)	Vol. NH_3 (cm^3/g)	Vol. NH_3 (cm^3/g)
SD-002	L	27	26	26
	H	6	6	6
SD-003	L	24	24	24
	H	6	6	6

Table 15. Results obtained from the TPD test of activated allophane.

Sample	Adsorption zone	Test 1	Test 2	Test 3
		Vol. NH_3 (cm^3/g)	Vol. NH_3 (cm^3/g)	Vol. NH_3 (cm^3/g)
SD-002	L	22	17	20
	H	4	4	4
SD-003	L	32	35	34
	H	1	2	2

3.2.7. Analysis of the TGA process curves

The analysis of the area under the curve of the thermogravimetric process was performed by the numerical integration method (Simpson 3/8), which is described by the Eqs 6 and 7 for the processes of light crude oil and asphalt.

$$I = \frac{3}{8}h[f(x_0) + 3f(x_1) + 3f(x_2) + f(x_3)] \tag{6}$$

$$h = \frac{b-a}{n} \tag{7}$$

where I = area under the curve; n = 3; a and b= limits of variation in mass; $f(x_i)$ = the time variation.

Using Eqs 6 and 7 and the mass and time data from Tables 12 and 13, the area under the curve of each of the catalysts used is obtained, including Asphalt and light crude oil without additives for each process. This is evidenced/shown in Tables 16 and 17 for light crude oil and Asphalt, respectively. The error percentage presented in each of the tables refers to the error obtained by comparing the result of the area under the curve between the Simpson method and the integration method by the regression obtained from the curves. Comparison of the areas below the curve for the 4 different cases. The case with lowest area value will be the most effective process.

Table 16. Values of numerical integration of the curves for light crude oil.

Curve	Area below the curve	% Error
Crude oil (25 ºAPI; 1.25%S) without catalyst	2257.61	1×10^{-4}
Activated allophane	2234.25	1.7×10^{-4}
Natural allophane	2178.78	0.98×10^{-4}
Commercial catalyst	2327.12	1.43×10^{-4}

Table 17. Values of numerical integration of the curves for asphalt.

Curve	Area below the curve	% Error
Asphalt (14 ºAPI; 2.6% S) without catalyst	1824.63	1.23×10^{-4}
Activated allophane	1924.61	$1{,}75 \times 10^{-4}$
Natural allophane	1704.66	1.87×10^{-4}
Commercial catalyst	1842.00	1.1×10^{-4}

Comparison of the areas below the curve for the 4 different cases. The case with lowest area value will be the most effective process.

3.3. Logistic regression analysis

The logistic regression method is commonly used to analyze the probability of occurrence of binary variables; this is achieved by adjusting the log probabilities (conditional probability) and the explanatory variables *(x)* to a linear model.

$$log\left(\frac{P(Y\ =\ 1|X)}{1\ -\ P(Y\ =\ 1|X)}\right)\ =\ \beta_0\ +\ \beta_1 X_1\ +\ \ldots\ +\ \beta_n X_n \tag{8}$$

where *Y = (0,1)* is the binary variable, *X = (X1, ..., Xn)* are "*n*" explanatory variables, and *β = (β0, ..., βn)* are the regression coefficients to be estimated on the database. In this work we used the software package *"R"* with the function "glm*"* and the packages "Rcmdr" and "Caret". The probability of occurrence is obtained according to the following logistic function: [21].

$$P(Y\ =\ 1|X)\ =\ \frac{1}{1\ +\ e^{-(\beta_0\ +\ \beta_1 X_1\ +\ \ldots\ +\ \beta_n X_n)}} \tag{9}$$

3.4. Method of maximum likelihood

This is a method of estimators calculation, which tries to find the value of the parameter for which the probability of obtaining the sample values is maximum [22]. In the method of estimation by maximum likelihood, the probability of the parameters and is constructed given a determined model for the observed empirical data. The likelihood function for a logistic model (Logit) is represented by the following equation [23].

$$\mathrm{L}\ =\ \prod_{i\ =\ 1}^{n} P_i^{Y_i}(1\ -\ P_i)^{1\ -\ Y_i} \tag{10}$$

taking the logarithm Neperian to the function of likelihood (Eq 10) we have:

$$lnL = \sum Y_i lnP_i + \sum(1 - Y_i)ln(1 - P_i) \quad (11)$$

The maximum likelihood estimation method chooses the estimator of the parameter that maximizes the likelihood function (*lnL*) (Eq 11), thus the procedure to be followed is to calculate the first order derivatives of this function with respect to the parameters we want to estimate, equalize them to 0 and solve the resulting system of equations Eqs 12 and 13.

$$\frac{\partial lnL}{\partial \widehat{\beta_0}} = \sum \left(Y_i - \frac{1}{1 + e^{-(\widehat{\beta_0} + \widehat{\beta} x_i)}}\right) = 0 \quad (12)$$

$$\frac{\partial lnL}{\partial \widehat{\beta}} = \sum \left(Y_i - \frac{1}{1 + e^{-(\widehat{\beta_0} + \widehat{\beta} x_i)}}\right) x_i = 0 \quad (13)$$

Next, we establish a particular model applied to the prediction of the catalytic effectiveness of the faujasite synthesized from the natural clinker, a dichotomous dependent variable *Ec*, which is a function of the optimal variables of the synthesis process called *th* (hydrothermal treatment time) and *n* (stirring speed), of the *BET* surface area, of the mass catalyst/crude mass ratio and crude properties, such as *°API* and % *S*.

$$E_c = \frac{1}{1 + e^{-(\beta_0 + \beta_1 \times th + \beta_2 \times n + \beta_3 \times API + \beta_4 \times S + \beta_5 \times R_{FC} + \beta_6 \times BET)}} \quad (14)$$

Equation 14 clearly indicates the function between the dependent variable *Ec* and the independent variables duly categorized in Table 18.

Table 18. Definition of variables for the logistic model.

Variable	Kind of variable	Symbology	Units
Hydrothermal treatment time	Independent	th	h
Stirring speed	Independent	n	rpm
°API	Independent	°API	°API
Percentage of sulfur	Independent	S	%
Relation: faujasite mass/crude oil mass	Independent	R_{FC}	g FAU/g crude oil
BET area	Independent	BET	m^2/g
Catalytic efficiency	Dependent (dichotomic)	E_c	-

Description of the variables used in the model with its respective unit and symbology, as well as the identification of the dependent variable.

3.5. Logistic regression model for catalytic efficiency using faujasite as catalyst

The logistic regression model obtained was based on the optimal ranges of the independent variables shown in Table 18 by means of experimental tests. It was considered that in these ranges the catalytic activity of faujasite for the cracking of light crude oil is efficient.

3.5.1. Experimental ranges

1. $18 \leq th \leq 24$

2. $1200 \leq n \leq 1400$
3. $10 \leq °API \leq 24$
4. $0.5 \leq S \leq 5$
5. $0 \leq RFC \leq 0.07$
6. $180 \leq BET \leq 362.16$

3.5.2. Optimal ranges

1. $23 \leq th \leq 24$
2. $1200 \leq n \leq 1300$
3. $16 \leq °API \leq 24$
4. $0.5 \leq S \leq 2$
5. $0.01 \leq RFC \leq 0.05$
6. $218.66 \leq BET \leq 362.16$

For the verification of the independent variables in the catalytic cracking process, they were evaluated with zeros if the variables were considered insignificant and ones if they were significant within the process. This analysis is shown in Table 19.

Table 19. Values of the independent random variables for faujasite.

Cases	th	n	°API	S	R_{FC}	BET	E_C
1	24	1200	18	1.2	0.021	347.75	1
2	18	1300	23	4.92	0.068	159.04	0
3	19	1300	22	4.28	0.059	169.67	0
4	24	1200	14	0.52	0.020	343.38	1
5	18	1200	24	1.5	0.062	159.47	0
6	24	1200	20	0.73	0.021	362.15	1
7	24	1300	18	0.94	0.022	235.80	1
8	18	1200	15	1.28	0.069	159.88	0
9	24	1400	23	0.57	0.023	252.24	1
10	18	1300	17	4.38	0.070	158.32	0

Table 17 shows the data on faujasite synthesis conditions, crude oil characteristics and the independent variables *RFC* and *BET*. It is necessary to establish a reference efficiency that matches the optimum ranges of the above-mentioned variables in order to determine an appropriate logistical model. The evaluation of the influencing variables for the logistic regression model by its level of significance is shown in Table 20.

Table 20. Influence of independent variables on catalytic efficiency. The discarded variables during the progressive runs are marked in green. The resulting influential variables are marked in red.

	Independent variable	Std. Error	z value	($Pr > \|z\|$)
First run	th	4.77×10^4	0.004	0.997
	n	7.44×10^2	−0.004	0.997
	ºAPI	1.01×10^4	0.003	0.998
	S	2.81×10^4	−0.002	0.998
	R_{FC}	2.55×10^6	−0.003	0.998
	BET	1.06×10^4	−0.004	0.997
Second run	th	0.38486	0.113	0.910
	ºAPI	0.26255	0.328	0.743
	S	0.82283	−1.027	0.304
	R_{FC}	74.4882	−1.316	0.188
	BET	0.01915	0.195	0.846
Third run	ºAPI	0.175939	0.615	0.538
	S	0.794851	−1.036	0.300
	R_{FC}	74.19592	−1.313	0.189
	BET	0.008451	0.672	0.501
Fourth run	S	0.819432	−1.042	0.2976
	R_{FC}	46.725874	−1.431	0.1524
	BET	0.005055	2.021	0.0433*
Fifth run	R_{FC}	4.243×10^1	−2.658	0.00786**
	BET	5.311×10^{-3}	1.990	0.04660*

*Note: The *R* program analyzes the variables that have an impact on the catalytic effectiveness, for this, it is observed in the last column that corresponds the degree of significance as long as the values of the variables approach 1 means that it does not influence the effectiveness therefore it begins to eliminate, as the variables are eliminated, the significance tends to zero. These are the variables that influence the process. The asterisks are provided by the program which indicates the variables with the highest degree of significance and therefore the variables that influence the process.

Different runs were calculated, until determining the significant variables. The stirring rate is discarded in the first run, because the experimental tests proved that it is less influential than the hydrothermal treatment time in the synthesis stage. The hydrothermal treatment time "*th*" in the second run is discarded, because the level of significance obtained from the "*R*" software is greater than 0.05. The variables: º*API* and % *S* are discarded in the third and fourth runs because the significance levels obtained from the "*R*" software are greater than 0.05. The variables *RFC* and *BET* are considered influential in the catalytic activity, because the levels of significance were smaller than 0.05.

Table 21 shows the coefficients associated with the independent variables influencing the catalytic efficiency obtained from the *R* software for the logistic regression model for faujasite.

Table 21. Coefficients for the logistic regression model of the faujasite.

Associated independent variable	Coefficient	Value
Intercept	β_0	1.474
R_{FC}	β_5	−130.3
BET	β_6	0.006974

Table 21 shows the values of the coefficients of the logistic regression model obtained from the program *R*, β_0 is the intercept or constant value of the logistic model, it represents the value that the dependent variable would take when the independent variable has no effect on the efficiency of faujasite catalysis.

From the values obtained in Table 19 we obtain the mathematical model of logistic regression for the catalytic efficiency of faujasite, represented in Eq 15.

$$E_c = \frac{1}{1 + e^{-(1.474 - 130.3 \times R_{FC} + 0.006974 \times BET)}} \tag{15}$$

Using the logistic regression model, the efficiency (prediction) and approximate to determine the validity of the model from the confusion matrix, which is presented in Table 22. The results are approximated to the reference efficiency by assigning the value of 1 for values greater than 0.5, otherwise as 0.

Table 22. Results of the application of the logistic regression model.

E_c (Reference)	E_c (Prediction)	E_c (Approximate prediction)
1	0.7619	1
0	0.0019	0
0	0.0065	0
1	0.7795	1
0	0.0041	0
1	0.7796	1
1	0.5626	1
0	0.0017	0
0	0.5588	1
0	0.0014	0

3.5.3. Evaluation of the logistic model using the confusion matrix

The accuracy of the logistic model was evaluated by the confusion matrix which was coded in *R* software, obtaining the results shown in Figure 15. The confusion matrix indicated a 90% accuracy of the logistic regression model for catalytic efficiency using faujasite.

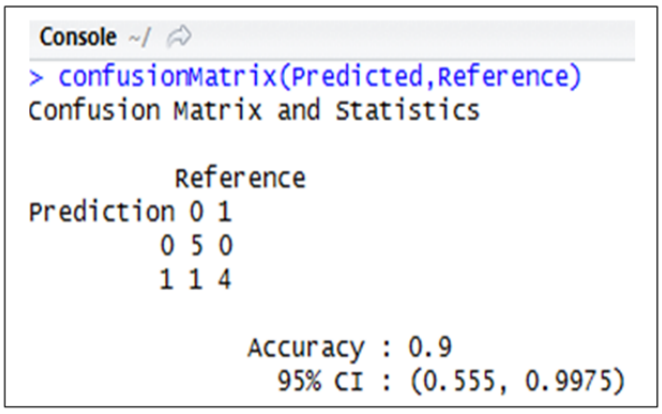

Figure 15. Encoding and results of the confusion matrix.

3.6. Logistic regression model for catalytic efficiency using allophane as catalyst

The obtaining of the logistic regression model was based on the optimal ranges of the independent variables illustrated in Table 16 by means of experimental tests. The allophane catalytic activity for the cracking of light crude and asphalt was considered in these ranges.

3.6.1. Experimental ranges

1. $12 \leq th \leq 30$
2. $700 \leq n \leq 1200$
3. $10 \leq °API \leq 26$
4. $0.5 \leq S \leq 5$
5. $0 \leq R_{FC} \leq 0.05$
6. $180 \leq BET \leq 460$

3.6.2. Optimal ranges

1. $17 \leq th \leq 18$
2. $750 \leq n \leq 800$
3. $14 \leq °API \leq 25$
4. $0.5 \leq S \leq 2.6$
5. $0.01 \leq R_{FC} \leq 0.05$
6. $254 \leq BET \leq 362.16$

For the verification of the independent variables present in the catalytic cracking process for allophane, they are valued with zeros if the variables were considered insignificant and ones if they were significant within the process. This analysis can be seen in Table 23.

The coding of the samples SD-001_18h, SD-002_18h, and SD-003_18h correspond to the activation with hydrotreatment time of 18 h and aging time of 24 h. The activated allophane samples correspond to samples with 18 h of hydrotreatment time and 72 h of aging time.

Table 23. Values of the independent random variables.

Case	Sample	Sample ID	BET	ºAPI	Si/Al	Sensor
1	Light crude oil	SD-001_18h	234	24.9	1.48	1
2	Asphalt	SD-001_18h		13.9		0
3	Light crude oil	SD-002_18h	192.2	24.9	1.9	1
4	Asphalt	SD-002_18h		13.9		0
5	Light crude oil	SD-003_18h	445.2	24.9	1.6	1
6	Asphalt	SD-003_18h		13.9		0
7	Light crude oil	Pure allophane	355.63	24.9	1.9	1
8	Asphalt	Pure allophane		13.9		1
9	Light crude oil	Activated allophane	445.2	24.9	1.6	1
10	Asphalt	Activated allophane		13.9		0
11	Light crude oil	Commercial catalyst	250	24.9	1.1	0
12	Asphalt	Commercial catalyst		13.9		0

Table 24 shows the coefficients associated with the independent variables influencing the catalytic efficiency of allophane obtained from the SPSS Software for the definitive logistic regression model.

Table 24. Logistic regression model coefficients.

Associated independent variable	Coefficient	Value	Std. Error	($Pr > \|z\|$)
Intercept	β_0	−545.754	123945.362	0.996
°API	β_1	9.627	2265.670	0.997
BET	β_2	0.217	62.266	0.997
Si/Al	β_3	185.397	44633.572	0.997

The logistic regression model depends on three variables: °*API, BET* area and *Si/Al* ratio. It coincides with the engineering perspective where °*API* is a process variable and the *BET* area is a nanotechnological variable.

From the values of the variables in Table 24 a mathematical logistic regression model is obtained for the catalytic efficiency of allophane:

$$E_c = \frac{1}{1 + e^{-(-545.754 + 9.627 \times API + 0.217 \times BET + 185.397 \times \frac{Si}{Al})}} \tag{16}$$

3.6.3. Evaluation of the logistic model using the confusion matrix

The accuracy of the logistic model for the catalytic effectiveness of allophane was evaluated by the confusion matrix in the SPSS Software. Figure 16 represents the confusion matrix in which the accuracy of the logistic regression model was obtained. The confusion matrix indicated 100% accuracy of the logistic regression model for catalytic efficiency using allophane.

This table visualizes that there are 12 samples of which 6 are efficient and 6 are inefficient, and the mathematical model correctly classifies these differences according to the explanatory variables.

Clasification table				
Predicted				
Observed		Censor		
		0	1	Rigth percentage
Step 1 censor	0	6	0	100,0
	1	0	6	100,0
Global percentage				100,0

Figure 16. Results of the confusion matrix.

3.7. Elasticity for independent variables influencing catalytic efficiency

Elasticity is the percentage change from one variable to the percentage change in another variable. Which are causally related by chemical physics.

Expressing as Z the linear sum of Eq 17

$$Z = \beta_0 + \beta_1 X_1 + \ldots + \beta_n X_n \tag{17}$$

$$E_C = \frac{1}{1 + e^{-Z}} \tag{18}$$

Clearing e^{-Z}

$$e^{-Z} = \frac{1 - E_c}{E_c} \tag{19}$$

We now derive Eq 14, representing the catalytic effectiveness, with respect to each independent influential variable:

model example of elasticity for catalytic effectiveness with respect to R_{FC}

$$\frac{\partial E_c}{\partial R_{FC}} = \frac{-1\left[e^{-(\beta_0 + \beta_1 \times th + \beta_2 \times \mathrm{n} + \beta_3 \times API + \beta_4 \times \mathrm{S} + \beta_5 \times R_{FC} + \beta_6 \times BET)}\right](-\beta_5)}{\left[1 + e^{-(\beta_0 + \beta_1 \times th + \beta_2 \times \mathrm{n} + \beta_3 \times API + \beta_4 \times \mathrm{S} + \beta_5 \times R_{FC} + \beta_6 \times BET)}\right]^2} \tag{20}$$

replacing Eq 18 in 20 we obtain the expression:

$$\frac{\partial E_c}{\partial R_{FC}} = \frac{\beta_5 e^{-Z}}{[1 + e^{-Z}]^2} = \beta_5 e^{-Z} \frac{1}{(1 + e^{-Z})^2} \tag{21}$$

replacing Eq 5 in 15 gives the following expression.

$$\frac{\partial E_c}{\partial R_{FC}} = \beta_5 e^{-z} E_c^2 \tag{22}$$

replacing Eq 15 in 18 gives the following expression.

$$\frac{\partial E_c}{\partial R_{FC}} = \beta_5 \left(\frac{1 - E_c}{E_c}\right) E_c^2 \tag{23}$$

$$\frac{\partial E_c}{\partial R_{FC}} = \beta_5 E_c (1 - E_c) \tag{24}$$

$$\varepsilon_{\frac{E_C}{R_{FC}}} = \frac{\frac{\Delta E_C}{E_C}}{\frac{\Delta R_{FC}}{R_{FC}}} = \frac{R_{FC}}{E_C} \times \frac{\partial E_C}{\partial R_{FC}} \tag{25}$$

replacing Eq 19 in 20

$$\varepsilon_{\frac{E_C}{R_{FC}}} = \frac{R_{FC}}{E_C}\beta_5 E_c(1 - E_c) = R_{FC}(1 - E_c)\beta_5 \tag{26}$$

$$\varepsilon_{\frac{E_C}{BET}} = BET(1 - E_c)\beta_6 \tag{27}$$

Table 25 shows the results of the elasticities of the independent variables *RFC* and *BET* as a function of efficiency, noting that there is a considerable change in efficiency by varying the amount of light crude oil or asphalt and faujasite.

Table 25. Elasticity results of influential variables.

$\varepsilon_{\frac{E_C}{R_{FC}}}$	$\varepsilon_{\frac{E_C}{BET}}$
−0.6516	0.578
−8.8438	1.107
−7.6378	1.176
−0.5746	0.528
−8.0455	1.108
−0.6031	0.557
−1.2537	0.719
−8.9758	1.113
−1.3223	0.776
−9.1079	1.103

In Figure 17, the equilibrium shows the convergence of the elasticities that diminish their minimum values and it is observed that efficiency is more sensitive to variation of the *RFC* variable.

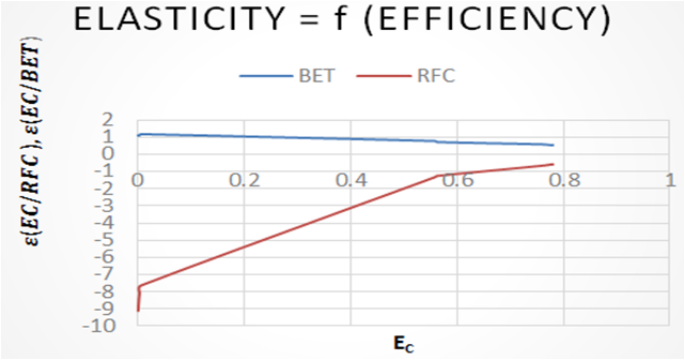

Figure 17. Graph of the elasticities of influential independent variables (R_{FC} y *BET*) as a function of catalytic efficiency.

3.8. Allophane used as asphalt additive

In Figure 18, the thermogravimetric analysis (TGA), it can be observed that for asphalt there is no loss of mass up to 238 °C, for 4% modified asphalt at 249 °C, for 5% modified asphalt at 250 °C and for asphalt modified at 6% at 153 °C, the previous results indicate an increase in matter from 25 °C to the indicated temperatures, this increase is not significant, which is interpreted as a result of the high sensitivity of the thermobalance until it reaches stability both thermal and physical. TGA diagrams results for different concentrations of allophane as asphalt additive.

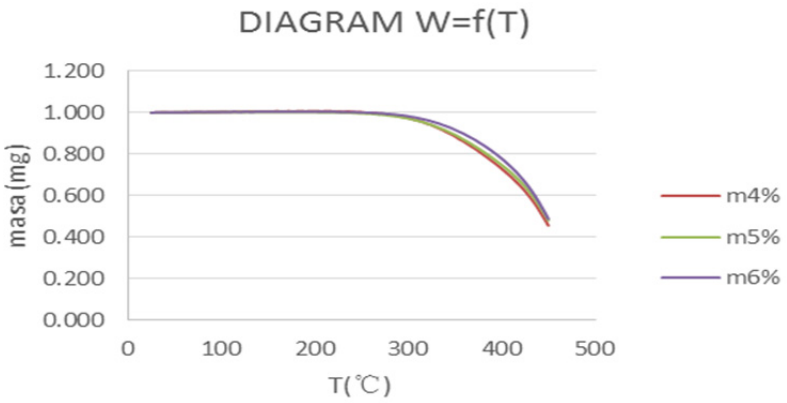

Figure 18. Mass diagram as a function of temperature for allophane as asphalt additive.

4. Discussion

The surface acidity of allophane and faujasite was modified by the ion exchange or desaluminization synthesis method (alkaline fusion method at 600 °C, followed by a treatment) managing to modify the Si/Al ratio.

Among the variables analyzed in the allophane activation process such as agitation speed, aging time, hydrotreatment time, NaOH/allophane ratio, the most important variables found are the aging time and the hydrotreatment time, since they define the amount of aluminum present in the allophane and this in turn establishes the Si/Al ratio, said ratio is a factor that influences the catalytic activity. By means of the chemisorption test, the acidity was determined by identifying the Lewis and Brøsnted sites in the samples, not all existing acidic centers can be considered as active development centers for the chemical reaction, but only a part of them will have strength enough acid to catalyze the reaction.

The thermogravimetry analysis was performed for samples of heavy crude oil, light crude oil and asphalt working at refinery conditions focused on the reaction temperature (420 °C), allowing to analyze the degradation of the samples, in this way the curves obtained through the results of analyzes reflect the phenomenon of degradation.

Atomic force microscopy (AFM) results are shown since the method used is non-contact to avoid contamination and damage of the sample, it is also specific for nanomaterials and real-scale topographic maps are obtained.

5. Conclusions

1. Faujasite is present according to the results of the FT-IR and XRD tests. The spectrum of the new FCC catalyst was taken as reference and, when compared to the synthesized faujasite spectrum, a peak of 569.6 cm^{-1} could be observed evidencing the presence of the typical double rings (D4R and D6R) for faujasite. In addition, the presence of a peak at 458.78 cm^{-1} indicated the presence of the supercage which also is characteristic of a faujasite type zeolite.

2. The most influential variable in the synthesis process of the faujasite from the natural clinker was the hydrothermal treatment time, obtaining 24 h as the optimal time of synthesis. By the X-ray diffraction test, up to 52.02% synthesized faujasite was determined at the optimum time of 24 h.

3. In the particle size test no particles smaller than 20 μm were detected. In addition the results of the BET surface area and pore volume tests for the synthesized faujasite were within the proper ranges of the acquired FCC catalyst.

4. The level of significance obtained is less than 0.05 for the independent variables RFC and BET. This suggests that faujasite is influential in catalytic activity. This level of significance used in the logistic regression model indicates that the RFC variable has a 99.9% acceptance over the BET variable.

5. The accuracy of the logistic regression model is at least 90%, according to the confusion matrix which verifies that the model is acceptable. Figure 17 shows that the elasticities of the influential variables RFC and BET tend to have a stable equilibrium of 0.02, obtained from the *"R"* software.

6. Samples of asphalt and modified asphalt meet the flash point requirements of NTE INEN 3030 (see Table 26) which helps storage of the product and transport conditions will not cause fires or explosions. Penetration according to NTE INEN 2515 (see Table 26) indicates that the allophane would help reduce the problems of sagging to 3 or 4% w/w adding to the asphalt, since it increases the hardness of the asphalt-allophane mixture. As for ductility, the best modified asphalt is that which has 6% w/w of allophane, this will remain cohesive against external deformations, such as ambient temperature or traffic deformations. The degree of performance for asphalt samples and for modified asphalts, for high temperatures the PG is 64 °C, in terms of the intermediate temperature, that is the failure temperature for the dynamic cutting module for samples aged in PAV is 22 °C for all samples tested. However, when looking at the results of the samples aged in RTFO (see Table 27) in detail, the allophane increases the operating temperature up to 70 °C, this test refers to the fact that once the asphalt folder has been inserted, the maximum working temperature for the asphalt of 3, 5 and 6% with allophane will be 70 °C, this is higher than the working temperature of asphalt samples without aging.

Table 26. Characterization results of asphalt and modified with allophane.

Requirement	Units		Original	Allophane percentage, %				Test standard	Reference norm
			AC-20	0	4	5	6		
Absolute viscosity at 60 °C	Pa·s	Min	160	270	306	304	388	ASTM D2171	NTE INEN 2515
		Max	240						
Penetration at 25 °C, 100 g, 5 s	dmm	Min	40	70	62	60	56	ASTM D917	NTE INEN 2515
		Max	-						
Flashpoint	°C	Min	232	265	272	278	281	ASTM D92	NTE INEN 3030
		Max	-						
Ductility	cm	Min	50	115.6	75.1	70.3	77.1	ASTM D113	NTE INEN 3030
		Max	-						
Softening point	°C	Min	48	49	51	50	50	ASTM D36	NTE INEN 2515
		Max	57						
Penetration rate	-	Min	−1.5	−64	−0.45	−0.79	−0.96	ASTM D5	NTE INEN 2515
		Max	1						
Dynamic cutting module, G*/senδ [(1)]	kPa	Min	1	1.3	1.71	1.57	1.58	ASTM D 7175	NTE INEN 3030
		Max	-						

*Note: Experimental specifications asphalt modified with alofan without aging. [(1)] Degree of performance: Expected range of good functioning of the asphalt binder, related to the average of the maximum temperatures of seven days and the minimum pavement temperature.

Table 27. Characterization results of asphalt and modified with allophane.

Research	Requirement	Units		Original	Allophane percentage, %				Test standard	Reference norm
				AC-20	0	4	5	6		
Trials in the thin film rotary kiln residue (RTFO)	Dynamic cut module, G*/senδ	kPa	Min	2.2	4.28	4.44	4.91	4.95	ASTM D7175	NTE INEN 3030
			Max	-						
	Penetration to 25 °C, 100g, 5 s	dmm	Min	-	42	41	40	40	ASTM D917	NTE INEN 3030
			Max	-						
	Softening point	°C	Min	-	58	58	59	59	ASTM D36	NTE INEN 3030
			Max	-						
	Penetration rate	-	Min	-	0.19	0.14	0.29	0.3	ASTM D5	NTE INEN 3030
			Max	-						
	Ductility	cm	Min	-	25	21	16.5	15	ASTM D113	NTE INEN 3030
			Max	-						
	Absolute viscosity at 60 °C	Pa·s	Min	-	1000	1170	1360	1410	ASTM D7175	NTE INEN 2515
			Max	1000						
Tests on the residue of the Pressure Aging Vessel (PAV)	Dynamic cut module, G*/senδ	kPa	Min	-	2480	2350	2670	2100	ASTM D7175	NTE INEN 3030
			Max	5000						
	Test temperature	°C		22					AASHT T315	NTE INEN 3030

*Note: Degree of performance: Expected range of good functioning of the asphalt binder, related to the average of the maximum temperatures of seven days and the minimum pavement temperature. Through a degree in the dynamic cut-off rheometer (DSR), the degree of performance equivalent to PG (64) was determined.

7. The pure allophane analyzed in the thermo gravimetric balance presented superior results compared to the commercial catalyst and activated allophane samples. This suggests that a different activation method than the one used for zeolites should be used in order to achieve better activation of allophane samples and thereby increase catalytic efficiency.

8. For the activation process of allophane, the optimal variables of the random process were those shown in Table 28.

Table 28. Optimal values of the variables for the activation of allophane.

Variable	Value
NaOH/allophane ratio	1.2/1
Calcination temperature	600 °C
Calcination time	1 h
Agitation speed	800 rpm
Agitation time	1 h
Water type 1/allophane ratio	5/1
Ageing time	3 d
Hydrotreating time	18 h

Considering that these variables are applied in the same way to the three pure samples to activate them and thus obtain the best results with these values.

Acknowledgements

To the research directorate of the Central University of Ecuador, project PRY-004 "Technical and economic feasibility of industrialization of allophanes and its use as a catalyst for the FCC fluidized catalytic cracking process" for the financing of this research, and the group of GIIP process research.

Conflict of interests

The authors declare no conflict of interest.

References

1. Centi G, Cambelli P, Perathoner S, et al. (2002) Environmental catalysis: trends and outlook. *Catal Today* 75: 3–15.
2. Degnan TF (2000) Applications of zeolites in petroleum refining. *Top Catal* 13: 349–356.
3. Pine LA, Maher PJ, Wachter WA (1984) Prediction of cracking catalyst behavior by a zeolite unit cell size model. *J Catal* 85: 466–476.
4. Arandes JM, Torre I, Azkoiti M J, et al. (2009) HZSM-5 zeolite as catalyst additive for residue cracking under FCC conditions. *Energy Fuel* 23: 4215–4223.
5. Madon R J (1991) Role of ZSM-5 and ultrastable Y zeolites for increasing gasoline octane number. *J Catal* 129: 275–287.

6. Chen NY, Garwood WE, Dwyer FG (1996) Shape selective catalysis, In: Heinemann H, *Shape selective catalysis in industrial applications*, 2 Eds., New York: Marcell Dekker, 62–136.
7. Chen NY, Degnan TF (1988) Industrial catalytic applications of zeolites. Chem Eng Prog 84: 32–41.
8. Ruthven DM, Post MFM (2001) Diffusion in zeolite molecular sieves, In: Bekkum H, Flanigen EM, Jacobs PA, et al, *Introduction to Zeolite Science and Practice*, 1 Ed., Amsterdam: Elsevier Science BV, 525–572.
9. O'connor CT, Van Steen E, Dry ME (1996) New catalytic applications of zeolites for petrochemicals. *Stud Surf Sci Catal* 102: 323–362.
10. Stoecker M (1994) Review on recent NMR results, advanced zeolite science and applications. *Stud Surf Sci Catal* 85: 429–507.
11. Avidan AA (1993) Origin, development and scope of FCC catalysis, In: Magee JS, Mitchell MM, *Fluid Catalytic Cracking: Science and Technology*, Amsterdam: Elsevier, 1–39.
12. Komvokis V, Tan LXL, Clough M, et al. (2016) Zeolites in fluid catalytic cracking (FCC), In: Xiao FS, Meng XJ, *Zeolites in Sustainable Chemistry*, Berlin: Springer, 271–297.
13. Levard C, Doelsch E, Basile-Doelsch I, et al. (2012) Structure and distribution of allophanes, imogolite and proto-imogolite in volcanic soils. *Geoderma* 183: 100–108.
14. Montarges-Pelletier E, Bogenez S, Pelletier M, et al. (2005) Synthetic allophane-like particles: textural properties. *Colloids Surf A* 225: 1–10.
15. Opfergelt S, Georg RB, Burton KW, et al. (2011) Silicon isotopes in allophane as a proxy for mineral formation in volcanic soils. *Appl Geochem* 26: 115–118.
16. Kaufhold S, Ufer K, Kaufhold A, et al. (2010) Quantification of allophane from Ecuador. *Clays Clay Miner* 58: 707–716.
17. Kaufhold S, Kaufhold A, Jahn R, et al. (2009) A new massive deposit of allophane raw material in Ecuador. *Clays Clay Miner* 57: 72–81.
18. Jimenez Calderón EH, Paucar A, Herrera P **(**2017**)** Study of the catalytic activity of the faujasite from natural clinker and pumice. *Phys Chem Indian J* 12: 1–16.
19. Kaufhold S, Dorhmann Z, Abidin Z, et al. (2010) Allophane compared with other sorbent minerals for the removal of fluoride from water with particular focus on a mineable Ecuadorian Allophane. *Appl Clay Sci* 50: 25–33.
20. Carrera Villamarín HM (2013) Evaluación y caracterización del catalizador del proceso de craqueo catalítico fluidizado (FCC). Ecuador Universidad Central del Ecuador. Available from: http://www.dspace.uce.edu.ec/handle/25000/2462.
21. Elío J, Crowley Q, Scanlon R, et al (2017) Logistic regression model for detecting radon prone areas in Ireland. *Sci Total Environ* 599: 1317–1329.
22. López R (2006) Variables aleatorias y función de probabilidades, *Cálculo de Probabilidades e Inferencia Estadística con tópicos de Econometría*, Cuarta Edición, Venezuela: UCAB, 37–64. Available from: https://books.google.com.ec/books?id=qWwR4jP8LlgC&printsec=frontcover#v=onepage&q&f=false.

23. Arnau J (1996) Técnicas de análisis avanzadas y diseños de investigación: Tendencias actuales y líneas futuras de desarrollo, In: Arce C, Arnau J, Ato M, et al., *Métodos y técnicas avanzadas de análisis de datos en ciencias del comportamiento*. Primera Edición, España: Edicions Universitat de Barcelona, 5–19. Available from: https://books.google.com.ec/books/about/M%C3%A9todos_y_t%C3%A9cnicas_avanzadas_de_an%C3%A1li.html?id=VXlz3-Sxuh4C&printsec=frontcover&source=kp_read_button&redir_esc=y#v=onepage&q&f=false.

AIMS Press